CHALMERS

Numerical Study of TEE Injection of Retention Chemicals in Semi Concentrated Pulp

Master of Science Thesis

KERSTIN OOM

Department of Chemical and Biological Engineering
Division of Chemical Engineering Design
CHALMERS UNIVERSITY OF TECHNOLOGY
Göteborg, Sweden, 2010

Numerical Study of TEE Injection of Retention Chemicals in Semi Concentrated Pulp

KERSTIN OOM

Examiner:

Professor Bengt Andersson, Chemical Engineering Design, Chalmers University of Technology

Supervisor:

Fredrik Fälth, Specialist, Modeling, Process R&D, Eka Chemicals, Bohus

Master of Science Thesis

Department of Chemical and Biological Engineering

Division of Chemical Engineering Design

CHALMERS UNIVERSITY OF TECHNOLOGY

Göteborg, Sweden 2010

Numerical Study of TEE Injection of Retention Chemicals in Semi Concentrated Pulp

KERSTIN OOM

Department of Chemical and Biological Engineering

Division of Chemical Engineering Design

Chalmers University of Technology

412 96 Göteborg, Sweden

Phone + 46 (0)31-772 1000

Printed: Chalmers University of Technology, Göteborg, 2010

Numerical Study of TEE Injection of Retention Chemicals in Semi Concentrated Pulp
Master thesis
KERSTIN OOM
Department of Chemical and Biological Engineering
Division of Chemical Engineering Design
Chalmers University of technology

Abstract

Retention chemicals are added to the pipe flow of pulp a few seconds before entering the headbox. Retention chemicals are added to attach the fines and fillers to the fibers to retain these small particles. The chemicals need to be well mixed in a few seconds since extended time and varying concentration can lead to unwanted side reactions. The flow of retention chemicals is small compared to the flow of pulp. The method with 90 degree side entry T-pipe nozzles will be studied as mixing device.

The purpose of this project is to get a better understanding of the mixing phenomenon by using Computational Fluid Dynamics. Effects of boundary conditions and rheology will be studied. The gained information should be used to easier determine appropriate injection flow rate and number of nozzles at existing plants.

A configuration with 4 holes is superior to 1 and 2 holes for pipes with 0.5m to 1m in diameter. The injection depth can be estimated by the momentum ratio even when the rheology of the suspension is considered. Turbulent properties of the flow are however more uncertain.

Keywords: Fiber suspension, Semi concentrated, TEE injection, Pipe, Crossflow, Computational Fluid Dynamics, Retention Chemicals

Preface

This master thesis was performed for Eka Chemicals to get a better understanding of the mixing of retention chemicals before the headbox. I am very grateful to my supervisor Fredrik Fälth, Specialist, Modeling, Process R&D, for his support and for giving me this very interesting task. His coworkers Johan Pettersson, Ronald Lai and Patrik Simonson have my gratitude for giving me a better insight in the process.

The work was performed at Chalmers University of Technology. I would like to thank my examiner Professor Bengt Andersson at Chalmers University of Technology for his great support and enthusiasm. Additionally I want to thank the PhD students Henrik Ström, Love Håkansson, Per Abrahamson and Andreas Lundström for their great support at any time. I am also thankful to Professor Anders Rasmuson for sharing some of his deep knowledge in fiber suspension flows.

Marko Hyensjö and Tomas Wikström at Metso, David Hammarström and Kati Lindroos at Processflow and Daniel Söderberg and Monika Fällman at the Royal Institute of Technology (KTH) deserves a gratitude. They have given me guidance through the large amount of available literature concerning fiber suspension flow and have inspired me through the working process.

Nomenclature

Greek letters

$\dot{\gamma}$	Rate of shear strain
ε	Dissipation rate
μ	Viscosity
ρ	Density
σ	Standard deviation
τ	Shear stress
τ_d	Time scale for dispersed phase
τ_{IC}	Inertial convective time scale
τ_T	Time scale for continuous phase
τ_{VC}	Viscous convective time scale
τ_{VD}	Viscous diffusive time scale
τ_y	Yield stress
υ_T	Turbulent viscosity
ω	Specific dissipation rate

English letters

A	Area
c	Coordinate (in this report)
C_D	Drag coefficient
C_{VM}	Virtual mass coefficient
D	Diameter

l	Length, momentum length
K	Consistency index
k	Kinetic energy
m	Mass
N	Crowding number
n	Consistency index
P	Pressure
r	Ratio
t	Time
U	Velocity
u	Velocity fluctuations
V	Volume
x	Mass fraction

Abbreviations

CoV	Coefficient of Variance
LDA	Laser Doppler Anemometer
PIV	Particle Image Velocimetry
RNG	Re-Normalization group
RSM	Reynolds Stress Model
UVP	Ultrasonic Velocity Profiler
WRV	Water Retention Value

1 Introduction

1.1 Background

Paper is produced by removing water from a pulp suspension. Most water is removed by draining in the forming section of the paper machine. To enhance the drainage, the pulp fibers are flocculated. For the papermakers it is desired to have a uniform paper and hence it is important that the created flocks are similar in size [1]. A uniform paper is important for the papers dry strength, because thick areas with large flocks mean that there also will be thinner areas in absence of these flocks. Adding retention aid can significantly contribute to uniformity in the formed paper, but the flocculation needs to be controlled by good mixing.

1.1.1 Flock creation and retention chemicals

Retention chemicals make the fines and fillers attach to the fibers. This prevents that these fine particles are lost, since they are too small to be retained by the filters used in the forming section of the paper machine [1]. Generally, both a nanoparticle solution and a polymer solution are therefore added before the screen[1]. If there is good mixing they can also be added after the screen but sometimes only nanoparticles are added after the screen. The chemicals should be well mixed with the pulp when it enters the headbox.

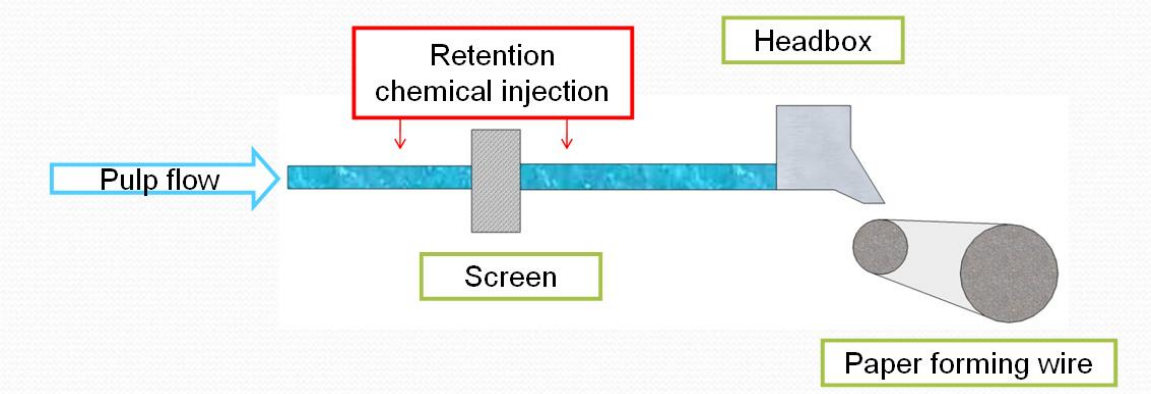

Figure 1-1: A very simplified picture of the process around the inlet to the paper machine.

The headbox is the inlet to the paper machine and it is followed by the forming section and the press section. These parts together are called the wet end. The task of the headbox is to distribute the suspension evenly across the wire at a constant velocity [4]. It is important that the headbox produces turbulent shear forces to break flocks and prevent formation of new flocks until the suspension is transferred to the wire. The shear is generated by friction in tubes and channels, or by changes in cross section. The velocity gradient which is perpendicular to the flow shears the flocks apart but it also makes the flocks and fibers rotate [1]. This rotation tends to bend the fibers and therefore it is an increased probability of interlocking between the fibers the

[1] Apparatus applied to screen the pulp to remove substances that has different shape and deformability compared to fibers. [344] The apertures in the device are either slots or round holes and the impurities to be rejected are passing through these apertures.

moment after. Hence it is a risk that the fibers will have time to reflocculate. A more persistent deflocculation can be achieved if the flocks are subject to extensional flow, meaning that the velocity gradient is parallel to the average flow. Extensional flow can for example be created by running the forming section faster than the velocity of the headbox jet. The optimal condition is to achieve bridging between fine particles and other surfaces that are strong enough to hold even when there is high shear in the system while bridges between pairs of fibers would become irreversibly broken at the same conditions.

The flow of chemical solution to inject is normally very small, especially compared to the flow of pulp that it shall be mixed with. If cold fresh water is used for the dilution of retention chemicals it results in that the energy loss is larger the more it is diluted since the cold water needs to be heated to the process temperature [2]. The reaction time of chemicals with fibers, fines and fillers is fast and therefore it is desired to reach good mixing within a few seconds [3]. Extended time and uneven concentration of chemicals makes it possible for unwanted side reactions.

One approach to distribute the chemicals is to introduce a static mixer in the pipe but then there is a risk for buildup of particles and fibers. Different configurations for jet injection have also been developed to increase the mixing. The simplest injection is to utilize 90 degree side entry T-pipe nozzles, but these are known to give inadequate mixing for reasonable flow ratios. The advantage with these simple nozzles is that the pipe stays smooth. No device is sticking into the pipe so the risk for clogging is minimized.

1.2 Objectives

It is desired to find the best configuration of injection pipes and injection flow rate for different flow rates and geometries of the main pipe to increase the result at existing plants. There is no limit for how small or large the flow rate ratio can be. It is a tradeoff between mixing result and dilution of the chemical solution. A good compromise between these factors is desired to be found.

Computational Fluid Dynamics is used to get a better understanding of the mixing properties. For evaluating the mixing it is of high importance to consider the effect of boundary conditions and the fiber suspensions rheology since these parameters are hard to estimate. The effect of number of injection points, flow ratio, injection pipe diameter and main pipe diameter will be studied.

1.3 Methods

A literature search in acknowledged databases and journals was made and specialists in fiber suspension flows both from the academic world and companies were contacted. The literature study was performed parallel to the simulations.

The simulations were performed in 3D with a symmetry plane and the mesh was generated in Gambit. Simulations where run in ANSYS Fluent 12.0, and models used were mainly the Standard-k-ε-model and the Reynolds Stress Model, but the RNG-k-ε-model was also tested.

To describe the rheology of the fiber suspension the Standard-k-ε-model was modified. In one model the molecular viscosity was modified and in the other the dissipation rate was reduced.

1.4 Limitations

- To simulate a fiber suspension as two separate phases with a multiphase model is computationally expensive since it requires a very fine mesh. Further multiphase models are not as verified as the single phase turbulence models. Therefore only single phase models will be used.
- Due to limitations in the measuring technique for rheological properties of pulp suspensions the attempts for a rheology model are very rough. Most simulations are run with properties of pure water and pure water is expected to be the closest approximation of the models. The two rheology models are used for a parameter study to conclude which parameters in the results which are more reliable and which are less.
- Injection of nanoparticles should be studied, but the complexity of the system makes it hard to consider its effect on the rheology. Therefore it is more of a general study of injection and mixing before the headbox.
- The retention chemical solution is assumed to be homogeneously mixed before injection.
- To reduce the computational cost a symmetry plane was introduced so only half the pipe was simulated.
- The injection pipes were simulated as holes with a flat velocity profile as inlet condition.
- Since the pipe is large (length 11m and width 1m) and the holes are as small as 5mm in diameter it is required to use size functions. The restrictions of the size functions resulted in problems with skewed cells and cells with high aspect ratio. It would have been possible to run the simulations with more cells but for a finer mesh the skewness of the cells became unacceptably high. The grid was instead refined in Fluent to see in what direction the results changed.

2 Theory

2.1 Turbulence

Turbulent eddies are created in the near wall region and when viscosity is not high enough to damp them, they can move across the pipe keeping the flow turbulent [5]. For the unstable character of turbulent flow to appear, the eddy velocity and the length to the nearest wall that can damp the turbulent fluctuations needs to be large compared to the viscosity. The Reynolds number gives a measure of the inertial resistance compared to the viscous resistance. An internal pipe flow becomes turbulent approximately when the Reynolds number exceeds 2100.

$$\mathrm{Re} = \frac{inertia\ \ forces}{viscous\ \ forces} = \frac{\rho UD}{\mu} \quad \textbf{(2-1)}$$

2.2 TEE injection in crossflow

TEE mixers are appropriate when dosing small streams into large streams. It can be one or more nozzles directed into the main flow. The simplest design is a jet that is directed perpendicular to the center line.

When deciding the optimal design of the system, there are several constraints [6]:

1. Flow rate ratio between main flow and injected flow

2. Pipe length available for mixing to occur

3. Flow pattern of the main fluid upstream of the injection point

4. Power requirements for the injection

5. Diameter of main pipe

Important for the mixing is the momentum ratio, r, between the injection and the main flow [7]:

$$r_{in,m} = \frac{l_m}{D_m} \quad \textbf{(2-2)}$$

Where l_m is the jet momentum length defined as:

$$l_m = \frac{D_{in}U_{in}}{U_m} \quad \textbf{(2-3)}$$

Inserting equation (2-3) in (2-2) yields:

$$r_{in,m} = \frac{D_{in}U_{in}}{D_m U_m} \quad \textbf{(2-4)}$$

If it instead would be the energy ratio

$$r_{energy} = \left(\frac{(1/2)m_{in}U_{in}^2}{(1/2)m_m U_m^2} = \frac{D_{in}^2 U_{in}^3}{D_m^2 U_m^3} \right) \quad \textbf{(2-5)}$$

that determines the penetration depth, a change in diameter or flow rate would give a different result. Therefore the design of the injection configuration becomes simpler if it can be verified what phenomenon that dominates concerning the penetration depth.

Generally when injecting retention aid chemicals, there is a problem that all chemicals stay near the wall because of the large pipe diameters and large flow rate ratios. With the momentum length it might be possible to identify the threshold velocity for when the jet penetrates into the bulk flow. Three regimes with very different mixing behavior are defined with this ratio [7, 8].

(1) **Wall-source regime** ($r_{in,m}$ <0.07): The jet is too weak to penetrate far enough into the pipe flow, but stays at the pipe wall and grows slowly. It is therefore not efficient mixing in this regime and hence not a desired operating condition.

(2) **Jet-mixing regime** ($0.07 < r_{in,m} < 1$): The jet penetrates into the bulk flow in the pipe. The jet then expands quickly due to the turbulent conditions in the pipe and there is efficient macro mixing [9].

(3) **Jet-impaction regime (**$r_{in,m} > 1.0$): The jet hits the opposite wall of the pipe. This impingement creates more efficient micro mixing [10] but it also gives a stress on the pipe wall if there is a strong impingement.

To get a measure of the penetration depth of the jet, it is appropriate to calculate the centre of mass in the coordinate in the direction of the injection.

Centre of mass: $\frac{\int (xc)dA}{\int (c)dA}$ **(2-6)**

where x is the mass fraction and c is the coordinate describing the distance from the injection hole in the direction of the coordinate. A is the cross-section of the pipe.

2.3 Mixing and reaction

To measure the degree of mixing the variance of the injected solution can be used. The Coefficient of Variance (CoV) is a regularly used measure of the degree of mixing and is defined as:

$$CoV = \frac{\sigma}{\bar{x}} \quad \textbf{(2-7)}$$

where the variance for a cross section is

$$\sigma^2 = \int \left(x^2\right) dA + \bar{x}^2 A \quad \textbf{(2-8)}$$

For the mixing of retention chemicals the following limits give a rough indication of the degree of mixing.

CoV<0.5	Fair
CoV<0.1-0.2	Good
CoV<0.05	Complete

In Fluent, the CoV is calculated for the average mass fraction in the cells. The CoV will hence not give any information of the mixing on scales below grid size, why the mixing time scales also need to be considered.

Mixing time scales

The inertial convective mixing is the deformation and stretching of large eddies into smaller eddies [5]. The inertial convective time scale is defined as

$$\tau_{IC} = \theta \frac{k}{\varepsilon} \quad \textbf{(2-9)}$$

The viscous convective time scale describes the mixing just above the Kolmogorov scale which represents the length of the smallest eddies in turbulent flow. For the viscous convective time scale both convection and viscosity are important.

$$\tau_{VC} = 17.25\sqrt{\frac{\upsilon}{\varepsilon}} \quad \textbf{(2-10)}$$

The time scale for mixing on the final stage is the viscous diffusive time scale

$$\tau_{VD} = \frac{\tau_{VC}}{0.303 + 17050 Sc^{-1}} \quad \textbf{(2-11)}$$

Reaction

To know at what rate the nanoparticles are attached to the fibers, the time scale for reaction and the time scales for mixing should be compared. The Dahmkoeler number is the ratio between relevant time scale for mixing and the time scale for reaction. Since the attaching of nanoparticles to the fibers is a physical mechanism of attraction of opposite charges it occurs very fast. The Dahmkoeler number will therefore be much larger than one and the mixing is the rate limiting step. This means that it is the time scales for mixing on different length scales that decides the distribution of nanoparticles. Fast mixing on small scales and slow mixing on large scales can thus give an uneven distribution on the fibers.

2.4 Rheology of fiber suspensions

Generally the mass fraction of fibers before the headbox is between 0.5%$_{mass}$ and 1%$_{mass}$. The mass fraction is a simple way to characterize a suspension but is not very informative of what flow properties the suspension has [11]. The volume fraction gives more information of how much the fibers are interacting. Other factors such as length and surface properties of the fibers and how bendy the fibers are also affect the degree of fiber interaction. The aspect ratio is the ratio between the length and the diameter of the fiber. A larger aspect ratio gives more entanglement between the fibers.

A measure of how much the fibers are interacting with each other can be given by the crowding factor [12]. This factor is used to define three regimes to characterize the flow properties.

$$N_{crowding} = \frac{C_v}{C_0} \quad \textbf{(2-12)}$$

where

$$C_0 = \frac{V_{cylinder}}{V_{sphere}} = \frac{3d^2}{2l^2} \quad \textbf{(2-13)}$$

and C_v is the volume concentration. C_v can be calculated as in equation (2-14) but this gives the volume concentration excluding lumen, which corresponds to a volume concentration for totally collapsed fibers.

$$C_v = \left(\frac{1}{\rho_f} + \frac{WRV}{\rho_v} \right) \rho_b C_w \quad \textbf{(2-14)}$$

WRV is the Water Retention Value and the indexes f, w and b means fiber, water and bulk.

There are three regimes based on the crowding factor [12]:

N < 1	Dilute regime
1 < N < 60	Semi concentrated regime
N > 60	Concentrated regime

In the dilute regime the interactions between the fibers can be neglected, in the semi concentrated regime there is forced collisions between the fibers and in the concentrated regime a fiber network is formed in the suspension [12]. Before the headbox the crowding factor is generally in the upper part of the semi concentrated regime [1, 13].

2.4.1 Measuring techniques

Many scientists have tried different methods to study the flow properties of fiber suspensions. One problem with the fiber suspension is that light cannot intrude through the fibers and hence the measuring depth is a limiting factor.

Optical methods

Optical measurement techniques can only measure a few mm for a 2-5%$_{mass}$ suspension.

PIV (Particle Image Velocimetry): Particles are introduced and pictures of the flow field are taken and then correlations are obtained for particle velocities.

LDA (Laser Doppler Anemometer): The fluid must be transparent to the used wave length of the laser beam. The interference when two laser beams meet is used in this measuring technique. When a particle passes through, a flashing frequency can be detected and this frequency gives the speed of the particle. LDA is however less limited than PIV since PIV has more problems with scattering of the light.

Acoustic methods

Measurements based on sound can measure deeper than the optical methods but are slower.

UVP (Ultrasonic velocity profiler): The time delay between transmitted and received signal gives the distance to the particle. Since it is acoustic it is a slow measuring technique with its limitations [14].

Sonar Doppler: This technique also has limitations in measuring speed since it is an acoustic method, but it is developing and the measuring speed has increased from 8Hz to 1000Hz [15]. This method can measure deeper than any of the other methods presented here but still it can only measure a few centimeters deep [16].

2.4.2 Flow properties

Fiber suspensions are known for their special flow properties. A concentrated fiber suspension behaves similar to a non Newtonian fluid [17]. A general correlation for non Newtonian materials is given by the Herschel-Bulkley model [14]

$$\tau = \tau_y + K\dot{\gamma}^n \qquad \textbf{(2-15)}$$

where τ is the shear stress, τ_y is the yield stress, $\dot{\gamma}$ is the rate of shear strain and the parameters K and n are consistency indexes. That a yield stress needs to be exceeded for the suspension to flow is due to the fiber network strength. For a Bingham plastic n=1. The Bingham model only works in a limited concentration interval and even in that interval it is a significant simplification of the flow [19]. With a rheology model it

is only an average that is simulated. In reality there is constantly formation and breaking of networks.

In pipe flow near the walls there are effects including orientation of fibers and compression of the continuous network leading to a decrease in the fiber concentration in this area. This affects the friction in the system and a friction loss appears which is due to a slip of the fiber phase that exists as a plug in the middle of the pipe. UVP measurements near the wall showed that the plug region decreased with decreasing consistency and increasing bulk velocity [14]. At sufficiently high velocity the flow becomes turbulent. In the schematic drawing of flow regimes presented in Figure 2-1 it is possible to see the decrease of the plug region and how the flow finally becomes completely turbulent.

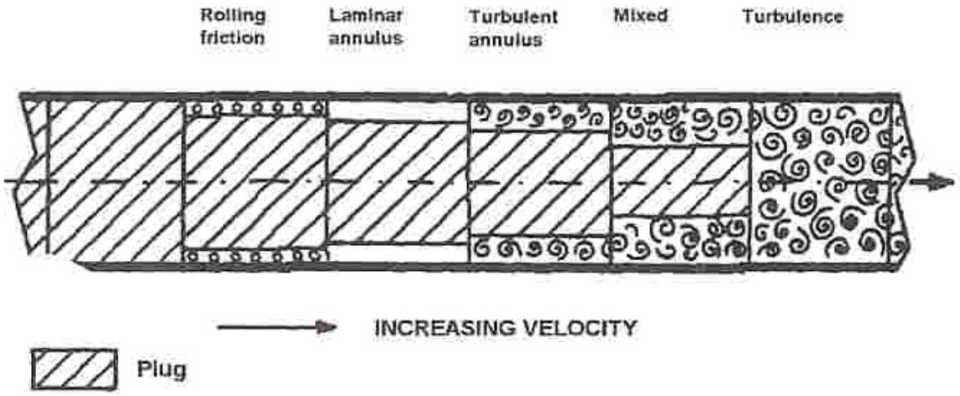

Figure 2-1: Flow regimes in pipe flow, [18]

Figure 2-2 shows another way to present different flow regimes in pipe flow. The positions of the regions depend on both the concentration and the characteristics of the fibers. The first regime, the plug flow regime, is laminar. In the second regime, the wall slip regime, the head loss decreases even though the flow rate is increasing. In the first part of the turbulent regime the pressure drop is lower than for water, but at increasing velocity the pressure head loss increases until the curve finally merges with the one for water [19]. According to this figure there is a certain slip of the fiber phase in a 1% $_{mass}$ pulp suspension. However, measurements are only performed up to 1m/s. Other measures performed on pipes with small diameter showed that the slip could be neglected for concentrations below 1%$_{mass}$ while there was a head loss for 1 - 2%$_{mass}$ suspensions [20].

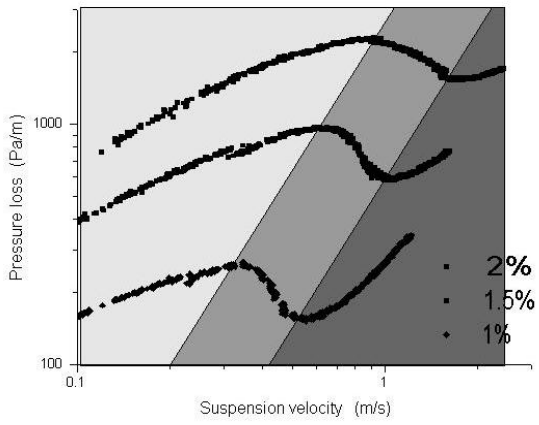

Figure 2-2: The plug flow regions for a birch pulp suspension. Light grey: Plug flow regime; Grey: wall slip regime; Dark grey: Turbulent flow regime [19].

Phase separation

Phase separation close to the pipe wall has been observed for both concentrated and dilute fiber suspensions. Experiments with PIV and UVP performed in suspensions with $1.9\%_{mass}$ and $2.7\%_{mass}$ fibers showed that the concentration was lower close to the walls. This gives a velocity profile that is very plug-like [14].

For a dilute suspension the concentration has showed to increase linearly from the wall into the bulk where it reached a constant value [21]. This was shown in a multiphase simulation where the fibers where assumed not to affect each other. It also corresponds to experimental data.

Apparent viscosity

One way to characterize the flow properties is to measure the apparent viscosity. In Figure 2-3 the apparent viscosity for pine is presented as a function of the mean shear rate [19].

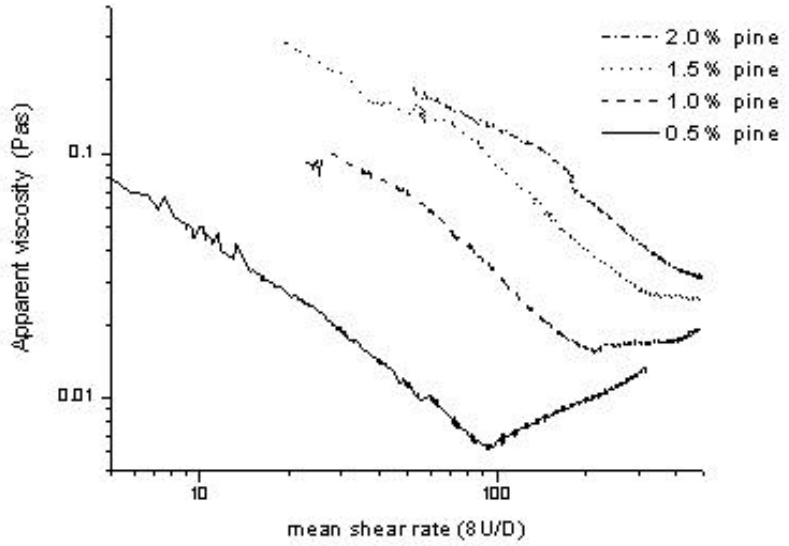

Figure 2-3: Apparent viscosity for a pine fiber suspension [22, 23]

2.4.3 Turbulence in fiber suspensions

The network strength in a suspension depends on the flow properties. At increasing shear rates the stresses become larger than the network strength and the flow becomes turbulent [16]. In turbulent flow the fibers are adjusted to the velocity field. Turbulent flow of fiber suspensions is acting more like water since the fibers are interacting less and the flow is said to be “fluidized” [19].

In turbulent flow particles both generate and suppress turbulence and the particles to be considered are both the fibers and the flocks [25]. Generation of turbulence is mainly due to a wake formed behind the particle. Suppression of turbulence is mainly due to that energy in the turbulent flow is transported to or absorbed by the particle. For example when the drag force acts on a particle in the turbulent flow energy is transported to the particle. Particles effect on the generation of turbulence is only significant if the particles are similar in size to the turbulent length scale or larger.

Due to the limitations in the acoustic measurement techniques there is a limited accuracy when measuring the velocity fluctuations in turbulent suspension. The higher Reynolds number the more demand on the speed of the measurement technique. Generally turbulence measurements are therefore performed in dilute suspensions with optical methods and if it is performed in concentrated pulp it is for relatively low Reynolds numbers since acoustic methods are needed.

Turbulence measurements with LDA were made for $0.5\%_{mass}$ pulp suspensions in pipe flow [26]. The fibers damped the turbulence compared to measurements in water. In one case the turbulence was damped 11-28% compared to pure water.

Four different measurements with LDA were performed on 1mm and 3mm long glass fibers in a suspension with concentrations around $0.1\%_{mass}$ and $1\%_{mass}$ [27, 28]. Turbulence was produced at length scales corresponding to the pipe diameter. However, for the short fibers at the low concentration turbulence was also produced on short length scales. This turbulence was assumed to be produced from rotation of the fibers since these fibers where able to move freely. It was found that the net effect for the case with long fibers of high concentration suppressed turbulence while the three other cases increased it.

This shows the complexity of how the fibers are affecting the turbulence. It is not possible to simply say that the turbulence is suppressed or increased since there are a lot of different length scales of the turbulent eddies and of the fibers and flocks.

Another example of the complexity of the suppression and generation of turbulence in fiber suspensions is measure of length scales in turbulent decay. In the case with water the short scales of motion died out, and after 32s only large scales of motion prevailed in a Newtonian fluid [29]. When turbulent energy decreases the viscous forces become stronger than the momentum forces at a larger scale compared to when there is more energy in the system. Therefore the dissipation occurs at larger scales. In pulp the small scales remains through the turbulent decay. Short fibers gave a larger effect than longer ones at constant crowding number. One hypothesis is that the large scale turbulence makes the fibers rotate and energy is hence taken from the large scale turbulence. The fibers rotation produces turbulence on a length scale similar to the fibers length scale. The net effect is a redistribution of energy from large to smaller length scales.

In pulp there is always a size distribution of the fibers, leading to that effects of both short and long fibers in combination will be apparent in the flow.

Quantitative turbulence measurements in $1\%_{mass}$ suspensions

The relative liquid-phase dissipation was measured for FBK (Fully Bleached Kraft pulp) fibers with a mass concentration of 1% [11]. The fibers length was between 0.25 and 4.5mm with most fibers below 0.5mm. The length weighted fiber length was 2.3mm where the long fibers were heavily weighted. The energy dissipation was measured by using mixing-sensitive chemicals. This results in that only the energy dissipated in the fluid phase is measured. Impellers are used to perform the mixing so the input energy is known. The results for the suspension were compared to water. The dissipation was lower in the water phase in the suspension than in pure water since energy is also dissipated in the fiber-phase through for example fiber-fiber friction. For FBK pulp in a high intensity mixer the relative dissipation rate can be approximated by equation (2-16). a is 52 ±6 with a 95% confidence interval [11].

$$\frac{\varepsilon}{\varepsilon_0} = \exp\left(-aC_V\right) \qquad \textbf{(2-16)}$$

This means that only a part of the energy is dissipated in the liquid phase and has resulted in mixing in the liquid phase. The rest of the energy has been lost to the fiber-phase at larger scales of turbulence than the Kolmogorov scale. This is possible because the fibers and the flocks are larger than the Kolmogorov scale.

Other measurements have been performed on fiber suspensions of 2.3mm long fibers with concentrations up to $1\%_{mass}$ and nl^3 (n is the number of fibers per unit volume and l is the length of the fibers) up to 6.7 [24]. The suspension is flowing in a rectangular channel with Reynolds numbers up to 92 000. The Reynolds number is based on the viscosity of water. PUDV (Pulsed Ultrasonic Doppler Velocimetry), which is an acoustic method, was used and hence inaccuracies caused by the slowness of the method needs to be kept in mind. The experiments showed that the dependency of the concentration decreased for increased Reynolds numbers both concerning velocity profile (Figure 2-4) and turbulent intensity (Figure 2-5).

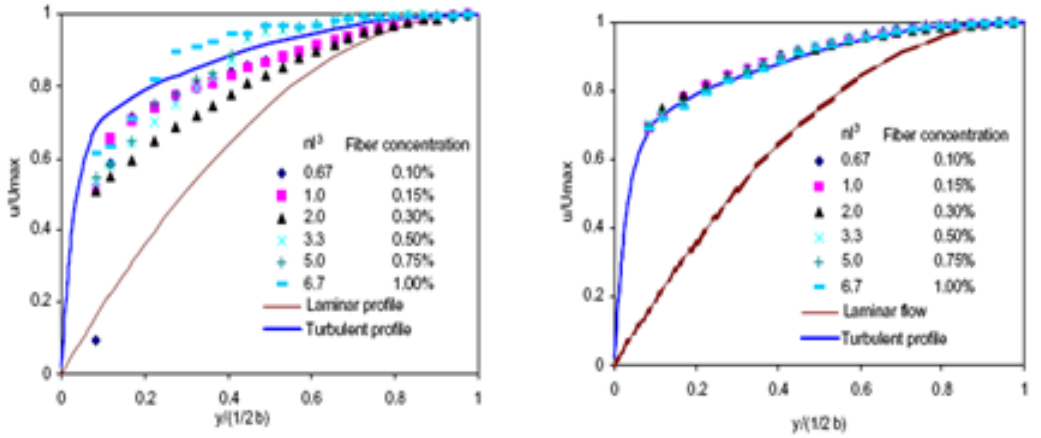

Figure 2-4: Velocity profile at Reynolds number of 12 000 (left) and 90 000 (right) [24].

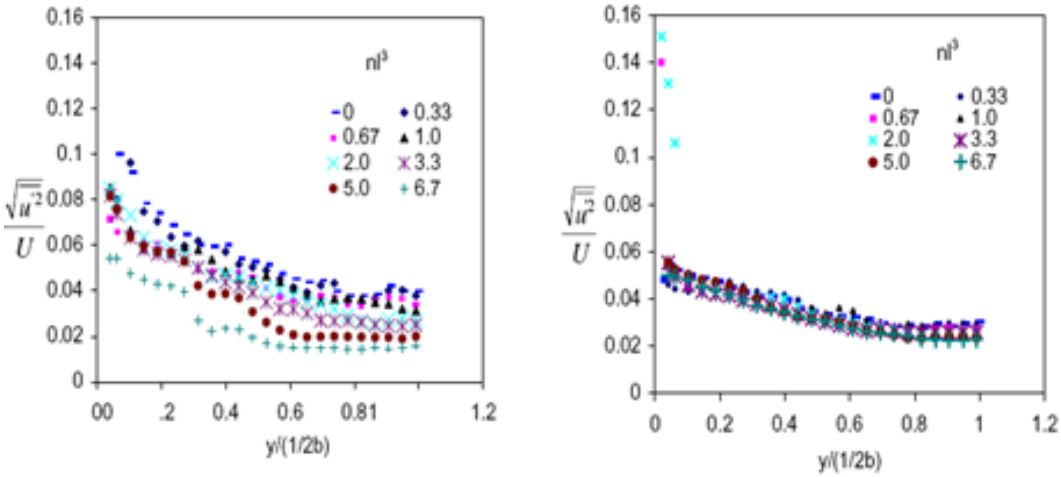

Figure 2-5: Turbulent intensity at Reynolds number of 37 000 (left) and 92 000 (right) [24].

2.4.4 Determining the flocks influence on the flow properties

After the retention chemicals are added there will be strong flocks, regions of large network strength. These flocks will be suspended in a phase of lower concentration

than before the addition of retention chemicals and that phase will hence be more "water like" than before.

To evaluate the effect of the flocks the turbulent Stokes number can be used [5]:

$$St_T = \frac{\tau_d}{\tau_T} \quad \textbf{(2-17)}$$

where τ_T is a relevant time scale for the continuous phase and τ_d is the time scale for the dispersed phase. When $St_T \rightarrow 0$ the particles follow the flow completely and when $St_T \rightarrow \infty$ the particles are not affected by the characteristics of the flow. If the Stokes number is larger than 1 the effect of the flocks on the flow cannot be neglected. The time scale for the dispersed phase can be calculated by a balance of forces acting on a single particle.

After the headbox flocks of sizes up to over 1cm can be expected. Before the headbox the flocks can be even larger since the shear in the headbox will reduce the flock size. However the turbulence in the pipe flow before the headbox will also shear the flocks resulting in a continuous forming and breaking of flocks. If the flocks held together by retention chemicals can be sheared apart by the turbulence in the pipe is however unknown. No size distribution has been found for the flocks and the size distribution is expected to vary much between different plants. A stochastic factor will also affect the size distribution.

2.5 Computational Fluid Dynamics

By using Computational Fluid Dynamics it is possible to get detailed information of the flow. The volume is divided into computational cells and the transport equations are solved numerically.

2.5.1 Governing transport equations

The material balance over a control volume described by the continuity equation is [5]

$$\frac{\partial \rho}{\partial t} + \frac{\partial \rho U_j}{\partial x_j} = 0 \quad \textbf{(2-18)}$$

The momentum balance which on its differential form is called Navier Stokes equation is:

$$\frac{\partial U_i}{\partial t} + U_j \frac{\partial U_i}{\partial x_j} = -\frac{1}{\rho}\frac{\partial P}{\partial x_i} - \frac{1}{\rho}\frac{\partial \tau_{ij}}{\partial x_j} + g_i \quad \textbf{(2-19)}$$

For single phase laminar flows the Navier Stokes equation can be solved directly but for turbulent flows it is necessary to use a model. The continuity equation is difficult to solve numerically. Therefore the continuity equation and the momentum balance are often combined in CFD software to form the Poisson equation for pressure which has more suitable numerical properties.

2.5.2 Turbulence models

The Reynolds decomposition is a simplification where instantaneous variables are split into a mean and a fluctuating part. [5] The flow is then described statistically by a mean flow velocity and turbulent quantities. All fluctuating parts are eliminated when taking the average in time except the nonlinear terms. These are called the

Reynolds Stresses and give the coupling between the mean and fluctuating part of the flow.

The Boussinesq eddy-viscosity approximation estimates the Reynolds stress tensor as proportional to the mean velocity gradients. Even in a pipe flow it is known that $\langle u_1^2 \rangle \neq \langle u_2^2 \rangle \neq \langle u_3^2 \rangle$. In turbulent pipe flow there are more velocity fluctuations in the flow direction, i.e. the eddies are slightly stretched in the flow direction. As a result there will be an underestimation of the velocity fluctuations in the flow direction of the pipe while the fluctuations in the direction perpendicular to the wall will be overestimated. Mixing in the near wall area thereby tends to be overestimated.

The Boussinesq approximation has some of the most notable failures when describing the following conditions [30]:

- Flows with sudden changes in mean strain rate
- Flow over curved surfaces
- Flow in ducts with secondary motions
- Flow in rotating fluids
- Three-dimensional flow

The standard k-ε model uses the turbulent kinetic energy and the energy dissipation rate to calculate the turbulent viscosity as given in the following equation.

$$\upsilon_T = 0.09 \frac{k^2}{\varepsilon} \qquad \textbf{(2-20)}$$

Further simplifications are introduced because the exact equations for k and ε are simplified. The standard k- ε model is known to give too high values for the dissipation in swirling flows and is therefore damping out vortices. In the RNG k-ε model this is corrected for by adding a source term in the ε-equation. Improvements for swirling flows and flows in curved geometries can then be expected, but for describing jets the RNG model is found to be less accurate than the standard k- ε model.

Stress Transport models have second moment closure; these models calculate the Reynolds stresses. However, for free shear flow they are not necessarily more accurate than two-equation models. Shortcomings in describing the round jet/plane jet anomaly carry through from two equation models to stress transport models. This is because the equation determining the scale e.g. ε or ω used by a stress transport model plays a key role also in the stress transport models.

Reynolds stress model (RSM) showed more compliance with experimental results for turbulent jets in cross flow than the standard k-ε model [31]. The mean velocity was well approximated by both turbulence models, but the k-ε appeared to overestimate the kinetic energy under present conditions. Even though RSM showed to be superior it still had results significantly different from experimental data.

2.5.3 Numerical aspects

The discretization schemes, 2nd order upwind and QUICK are unbounded but fulfills the transportiveness criterion [5]. Since they are unbounded they can give rise to numerical problems in areas with steep gradients. The 1st order upwind scheme is

bounded and fulfills the transportiveness criterion. A drawback is that the transport of entities is overestimated. This is called numerical diffusion and it is reduced by a finer mesh.

QUICK which is of 3rd order might give better accuracy for swirling and rotating flows than 2nd order upwind do [32]. Generally 2nd order upwind is sufficient and QUICK will not give any significant improvement in accuracy. QUICK can only be used for hexahedral and quadrilateral cells so when this scheme is used 2nd order will be used for all other cells.

A structured mesh compared to an unstructured mesh gives less numerical problems and lower numerical diffusion. Highly skewed cells should be avoided since they can decrease accuracy and make the solution unstable [32].

3 Methods

3.1 Mesh

Different meshes were created for different geometries and flow rates. The mesh that has been used in most simulations is shown in Figure 3-1. The diameter of the pipe is 1m, the length is 11m and the diameter of the injection holes is 10mm. The mesh is created for a flow rate of 2m/s. The boundary layers are created to get a y+ value below 100 in the simulations. If water is simulated at these conditions it corresponds to a Reynolds number of approximately 2 000 000.

a)

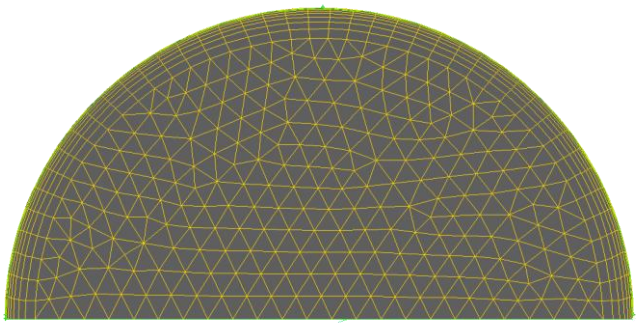

b)

Figure 3-1a and b: Mesh for the base case

An injection zone 0.9m to 1.1m from the inlet was created. In this volume the T-Grid scheme was used and a size function growing from the injection holes into the volume was used. The rest of the volume consisted of structured cells created by the Cooper

scheme. All meshes passed the grid check in Gambit with a maximum equisize skew of 0.97. The mesh created for the base case consisted of 200 000 cells before refinements. Simulated cases were generally refined up to 300 000 to 400 000 cells.

3.2 Convergence and accuracy

The QUICK scheme could not be used for the flow field due to problems with convergence. Instead the 1st order upwind scheme was used. The mesh is structured in the main parts of the volume, which reduces the numerical diffusion. QUICK could be used for species which is most important since it reduces the numerical diffusion of species.

Scaled residuals were generally set to be lower than $1 \cdot 10^{-6}$ but it could rarely be reached for species. The scaled residual for species was generally in the range $1 \cdot 10^{-4}$ - $1 \cdot 10^{-3}$ when it leveled off. This was for an initial condition of a fully developed turbulent profile in the whole pipe. The continuity was also checked to see that convergence was reached.

3.3 Models

3.3.1 Viscous model choice for jet injection in water

The Standard k-ε-model was the first choice of model and was run for all tested conditions. It was chosen since it is stable and known to be better for describing jets than the RNG k-ε-model. However, the RNG k-ε-model was also tested since it better describes swirl than the Standard k-ε-model does.

The RSM is expected to give the most accurate results of the models used, since a pipe flow with jet injection is anisotropic and due to the model's compliance with experimental results presented in 2.5.2. However, RSM is more computationally expensive and less stable than the standard k-ε-model but will be used in as many cases as possible.

3.3.2 Models for describing the fiber suspension flow

When describing the rheology of the fiber suspension only the Standard k-ε model was used since this is a stable model and therefore simpler to modify. The rheology models are for describing a $1\%_{mass}$ suspension.

Reduction of the dissipation rate

This model is based on the knowledge of relative liquid-phase dissipation rate presented in chapter 2.4.3. Equation 2-16 gives the relative liquid-phase dissipation of 44% for a volume concentration of 0.016. To describe the damping of ε, the ε-equation in the standard k-ε model was modified.

$$\frac{\partial \varepsilon}{\partial t} + \langle U_j \rangle \frac{\partial \varepsilon}{\partial x_j} = C_{\varepsilon 1} \nu_T \frac{\varepsilon}{k} \left(\left[\frac{\partial \langle U_i \rangle}{\partial x_j} + \frac{\partial \langle U_j \rangle}{\partial x_i} \right] \frac{\partial \langle U_i \rangle}{\partial x_j} \right) - C_{\varepsilon 2} \frac{\varepsilon^2}{k} + \frac{\partial}{\partial x_j} \left(\left[\upsilon + \frac{\nu_T}{\sigma_\varepsilon} \right] \frac{\partial \varepsilon}{\partial x_j} \right) \quad \textbf{(3-1)}$$

Accumulation + convection = produced – dissipated + diffused

The production of ε was increased by increasing the constant $C_{\varepsilon 1}$. Increasing $C_{\varepsilon 1}$ leads to more production of ε resulting in a sink in k (the kinematic energy). Since k is

reduced the turbulent viscosity is reduced. The reduction in k also leads to a reduction in ε since ε is the dissipation of energy and there is less energy to dissipate when the turbulence is damped. The term describing the dissipation of ε depends on ε^2 and therefore the dissipative term in the equation will also increase and the balance will be found. It is therefore not necessary to increase the constant $C_{\varepsilon 2}$ to find balance.

A dissipation rate of 44% was reached with $C_{\varepsilon 1}$ = 1.88. The turbulent viscosity has then decreased to a eighth compared to for water. Since the energy in the suspension will be taken from all different length scales in the energy cascade, the kinetic energy in total will not be halved. To in a one phase model simulate ε as around half as large is a worst case scenario to use for the parameter study.

Model based on apparent viscosity

In Figure 2-3 the apparent viscosity for a $1\%_{mass}$ suspension is presented. It gives an apparent viscosity of 0.14 for the simulated system (D_m=1m and U_m=2m/s). This corresponds to a Reynolds number of approximately 14 000. Simulations with this apparent viscosity for the whole pipe led to a pressure drop that is six times larger than for water. Too much energy is then added to the system and the mixing is overestimated. This is not reasonable since the pressure drop for a fiber suspension pipe flow is smaller or similar to the pressure drop for a water pipe flow.

Simulations were instead run with a viscosity depending on the distance to the pipe wall. Close to the wall the viscosity is $1.003 \cdot 10^{-3}$ (the viscosity of water) 1.5 mm from the wall it increases linearly to 0.14 Pas which is reached 2.5 mm from the wall. In Figure 3-2 it can be seen how the viscosity varies along the radius of the pipe. The pressure drop is still higher than for water so the turbulent properties will not be representative. The model will mainly be used to see if the viscosity affects the penetration depth of the injected flow.

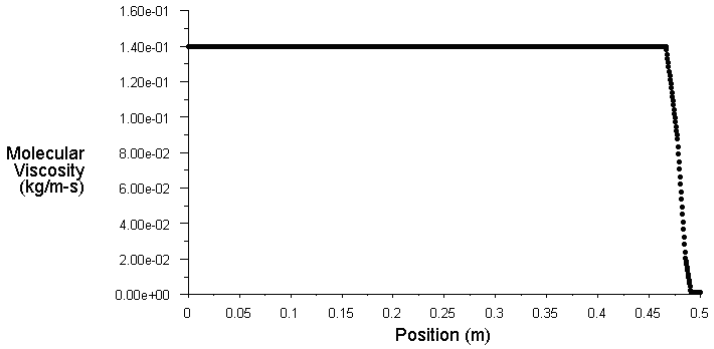

Figure 3-2: How the molecular viscosity varies along the radius in the rheology model

3.4 Performed studies

The following studies were performed.

3.4.1 Effect of boundary conditions and model

Eleven chosen cases were tested to evaluate the effect of different boundary conditions. Many of the cases are extreme with either high or too low injection velocity.

Cases	Main flow rate [m/s]	Main pipe diameter [m]	Feed flow rate [m/s]	Feed flow diameter [mm]	No. of feed points	Main/feed flow ratio
Case 0	2	1	6.25	10	1	3200
Case 1	2	1	62.5	10	1	320
Case 2	6	1	6.25	10	1	9600
Case 3	2	1	3.125	10	2	3200
Case 4	2	1	31.25	10	2	320
Case 5	2	1	1.5625	10	4	3200
Case 6	2	1	15.625	10	4	320
Case 7	2	1	25	5	1	3200
Case 8	2	1	6.25	5	4	3200
Case 9	2	1	10	25	1	320
Case 10	2	0.5	6.25	10	1	800

Table 3-1: Conditions for tested cases.

The list below shows the working process for each case in table 3-1.

1. Simulating:
   Standard k-ε model with "standard boundary conditions"[2] and flat inlet profile.
2. Simulating
   Standard k-ε model with an inlet profile of a fully developed turbulent flow.
3. Refinements for (2)
4. Simulating:
   Reynolds stress model with an inlet profile of fully developed turbulent flow.
5. Refinements for (4) to see if the results changed in the same direction as for (2).

The inlet profile for (2) and (4) was created by writing the values of k, ε and u from a plane close to the outlet before injection was introduced and using these values as inlet conditions. This was repeated until steady state was reached. It took approximately 30 to 40 meters for fully developed turbulence to appear.

3.4.2 Velocity study

Validate momentum ratio

The threshold velocity between the wall source regime and the jet injection regime was calculated for varying geometries to verify if the momentum force is dominating.

$$U_{in} = \frac{0.07 U_m D_m}{D_{in}} \qquad \textbf{(3-2)}$$

A constant of 0.15 was also used to see if the momentum ratio applies for higher velocities as well.

Optimization of injection velocity and number of holes

Simulations with varying velocity and number of injection points were run with water, modified viscosity and reduced dissipation rate. It was a parameter study to see the

[2] Turbulent intensity of 5.4% and turbulent length scale of 0.07

uncertainty in the results. The general geometry used was a pipe with a diameter of 1m. A velocity study was also performed for a pipe with a diameter of 0.5m.

For 4 holes it was seen that at a certain injection velocity the CoV increased with increasing velocity. By looking at the velocity field it was seen that the velocity fields around each injection point damped each other's rotation. Because of this a more stagnant zone in the middle appeared where the injected fluid was stacked up. Therefore different velocities for different holes were tried, but with no improved results.

Refinements were made for a part of the simulations to see in what directions the results changed. The mesh was first refined in the velocity gradient without injection and a new profile was saved and used, and the mesh was refined in the velocity gradient with injection. It was also refined in the mass fraction gradient.

3.5 Stokes number calculations

Turbulent properties such as k, ν_T and ε were taken from simulations and corresponding length- and time scales were calculated.

The Kolmogorov length scale was compared to the fiber length. It is not necessary to calculate the Stokes turbulent number for the fibers since these are much smaller than the turbulent length scale. However, Stokes number was calculated for 3 different flock diameters; 5mm, 10mm and 15mm.

When setting up the mass balance only the drag force and the virtual mass force were accounted for, which resulted in the following equation [5].

$$m_d \frac{dU_{i,d}}{dt} = \frac{1}{2} A_d C_D \rho \left|U_f - U_d\right| \left(U_{i,f} - U_{i,d}\right) - C_{VM} \rho_f V_d \frac{D_d}{D_f} \left(U_{i,f} - U_{i,d}\right) \quad \textbf{(3-3)}$$

The second term on the RH side is the virtual mass force which comes from the acceleration or deceleration of the surrounding fluid. C_{VM} is usually around 0.5. If the densities are approximated to be equal the expression becomes

$$1.5 m_d \frac{dU_{i,d}}{dt} = \frac{1}{2} A_d C_D \rho \left|U_f - U_d\right| \left(U_{i,f} - U_{i,d}\right) \quad \textbf{(3-4)}$$

According to [34]

$$\frac{dU_{i,d}}{dt} = \frac{\left(U_{i,f} - U_{i,d}\right)}{\tau_d} \quad \textbf{(3-5)}$$

Inserting equation (3-5) in (3-4) gives the time scale of the dispersed phase

$$\tau_d = \frac{1.5 m_d}{\frac{1}{2} A_d C_D \rho \left|U_f - U_d\right|} \quad \textbf{(3-6)}$$

The maximum relative velocity is if the flock is unaffected by the flow and it can be approximated as

$$\left|U_d - U_c\right| = \sqrt{k} \quad \textbf{(3-7)}$$

The relative velocity can hence be between 0 and $\sqrt{k}$.

The relative Reynolds number was calculated accordingly

$$\mathrm{Re}_d = \frac{d_p \rho |U_d - U_c|}{\mu} \quad \textbf{(3-8)}$$

The density of the flock was approximated to 1200kg/m^3 since water has a density of 1000kg/m^3 and the fibers has a density around 1500kg/m^3. Re_d was between 500 and 3000 for the flocks.

The drag coefficient was then approximated to 0.4 from Figure 3-3. As can be seen measurements of the drag coefficient can vary significantly.

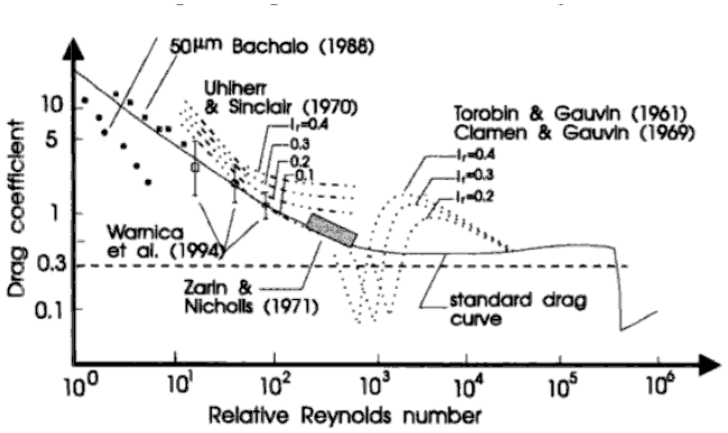

Figure 3-3: Drag coefficient measured for varying relative Reynolds numbers [33]

The time scale for the particle is then compared to the time scale of the largest eddies, i.e. the turbulent time scale [34].

4 Results

4.1 Data of flow properties

Turbulent properties

Turbulent properties for the different rheology models are presented in the two tables below. It is a cross-section average for simulations with fully developed turbulence and without injection. Therefore the values are the same for any cross-section along the pipe.

Rheology	Mesh	k [m^2/s^2]	ε [m^2/s^3]	ν_T [kg/ms]
Water	Base mesh	0.011	0.023	2.2
Water	For case 2	0.085	0.536	5.8
Water	For case 10	0.013	0.056	1.2
44% ε	Base mesh	0.0033	0.011	0.27
0.001-0.14 Pas	Base mesh	0.030	0.010	2.3

Table 4-1: Turbulent properties

Rheology	Mesh	η [mm]	l [mm]	τ_{IC} [s]	τ_{VC} [s]	τ_{VD} [s]
Water	Base mesh	0.081	52	0.25*	0.22	0.0065
Water	For case 2	0.037	46	0.079*	0.024	0.0014
Water	For case 10	0.065	27	0.12*	0.073	0.0042
44% ε	Base mesh	0.098	17	0.19*	0.13	0.0074
0.001-0.14 Pas	Base mesh	0.056	52	0.15*	0.054	0.0031

Table 4-2: Length scales and time scales of the turbulent flows. * represents the limiting time scale.

The flocks are generally smaller than the large energy containing eddies which are around 50mm. This implies that the flocks' effect on the flow can be neglected. However, calculations for the Stokes number were still performed. Time scales for the dispersed phase, $\tau_{D,}$ can be seen below. τ_D can is then divided by the turbulent time scale, which is in the interval 0.2 - 0.5s, to get Stokes turbulent number.

Tested flock sizes [mm]	5	5	10	10	15	15
Relative velocity [m/s]	0.33	0.15	0.33	0.15	0.33	0.15
τ_D [s]	0.1	0.2	0.2	0.4	0.3	0.6
S_T	0.2 - 0.5	0.4 - 1	0.4-1	0.8 - 2	0.6 - 1.5	1.2 - 3

Table 4-3: Time scale of the dispersed phase for different flock sizes and relative velocities.

Pressure drop

Model	Pressure drop (Pa)
Water	220
44% dissipation rate	96
0.001 to 0.14 Pas viscosity	232

Table 4-4: Pressure drop over the pipe

4.2 Effects of boundary conditions

CoV was calculated for a cross section 10m downstream of the injection. The simulations with standard boundary conditions had CoV significantly different for the simulations with developed inlet profile. The worst case was case 1 with 29% lower CoV than corresponding simulation with developed inlet profile. The other cases ranged from 3% to 29% deviation with an average deviation of 12%.

4.3 Validation of momentum ratio correlation

Penetration depth and spreading of the jet for different geometries are presented in Figure 4-1 and 4-2. The coefficient of variance for the same simulations can be viewed in Figure 4-3. The injection velocity is set to the threshold velocity calculated by equation (3-2). What the different series stand for is presented in Table 4-5.

Series	D_m [m]	U_m [m/s]	D_{in} [mm]	U_{in} [m/s]
A	0.5	2	10	7
B	1	2	5	28
C	1	6	10	42
D	1	2	25	5.6
E	1	2	10	14

Table 4-5: Geometry for the different series.

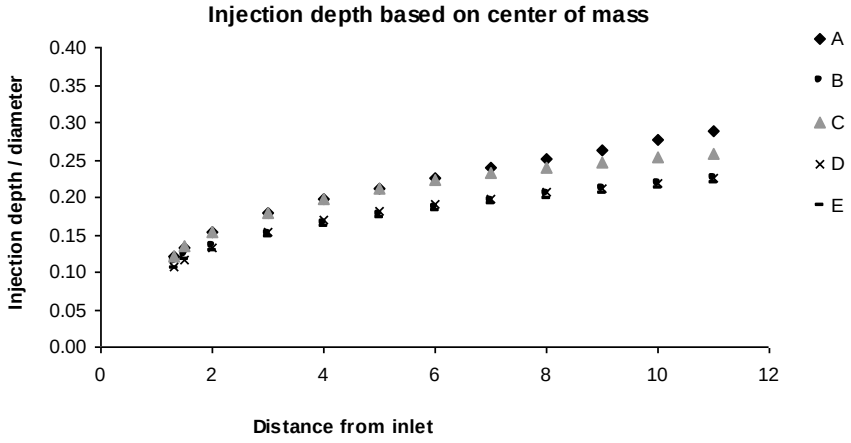

Figure 4-1: Centre of mass at the threshold velocity for different geometries and main flow rates.

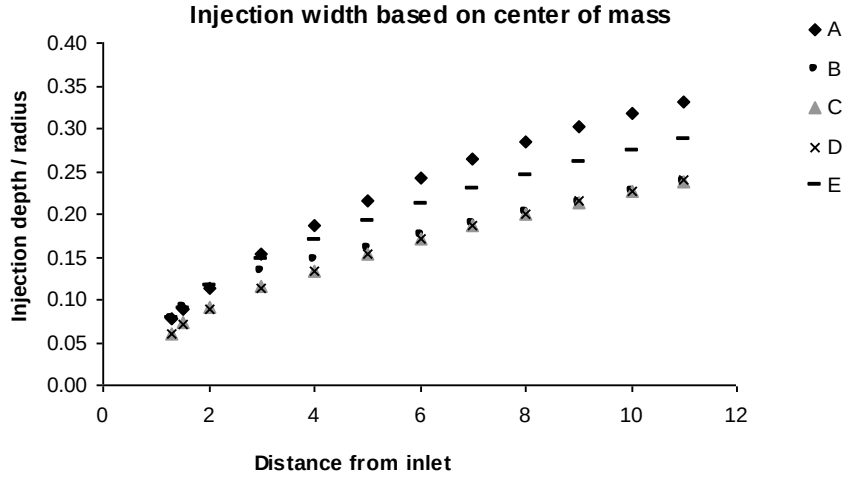

Figure 4-2: Centre of mass at the threshold velocity for different geometries and main flow rates.

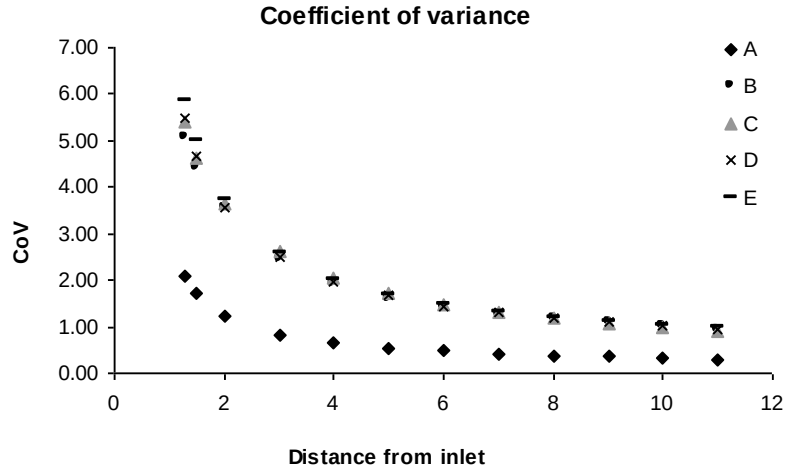

Figure 4-3: CoV at the threshold velocity for different geometries and main flow rates.

Rheology model dependency

A parameter study of the effect of the different rheology models at the threshold velocity (calculated by equation 3-2) is presented in Figure 4-4 to 4-6.

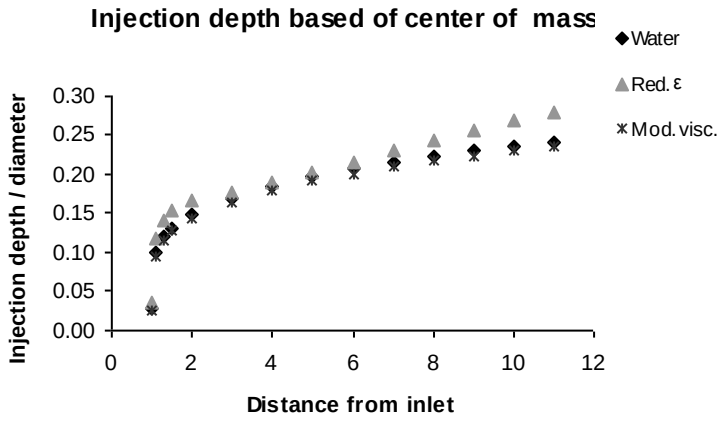

Figure 4-4: Centre of mass at the threshold velocity for different rheology models

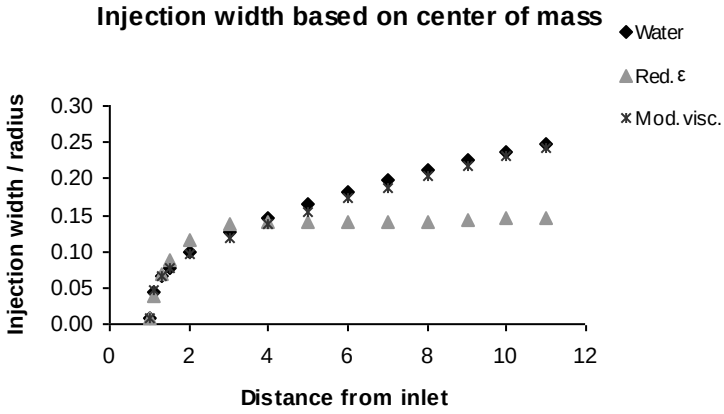

Figure 4-5: Centre of mass at the threshold velocity for different rheology models

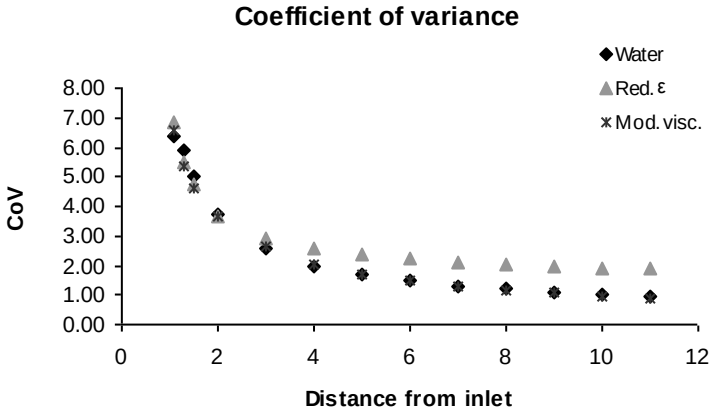

Figure 4-6: CoV at the threshold velocity for different rheology models

There was a question if the viscous forces would affect the injection depth more at lower velocities. Figure 4-7 shows a comparison of the model with modified viscosity and the model with water for low injection velocities.

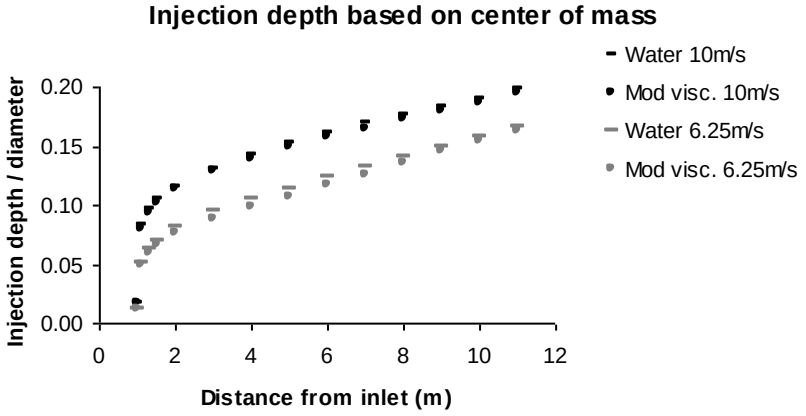

Figure 4-7: Injection depth for different injection velocities. A comparison of the model with modified viscosity and simulations with water.

4.4 Study of injection velocity and number of injection points

Velocity studies for systems with water for different geometries are presented in Figure 4-8 to 4-10. The flow rate ratio is the total injected volume flow divided by the total volume flow in the main pipe. The CoV is calculated from a cross section 10m downstream of the injection. Notice the different scales on the axes if comparing the three pictures with each other.

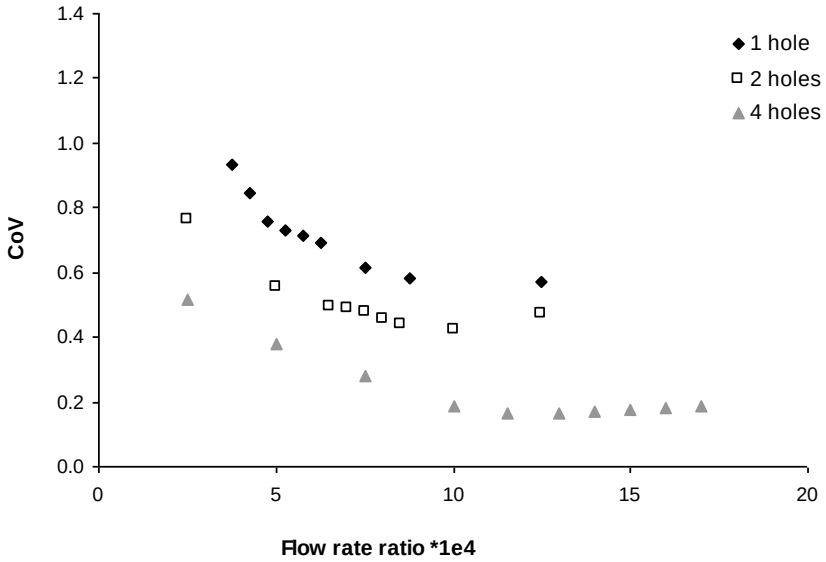

Figure 4-8: Coefficient of variance for a pipe with D_{in}=5mm and D_m=1m

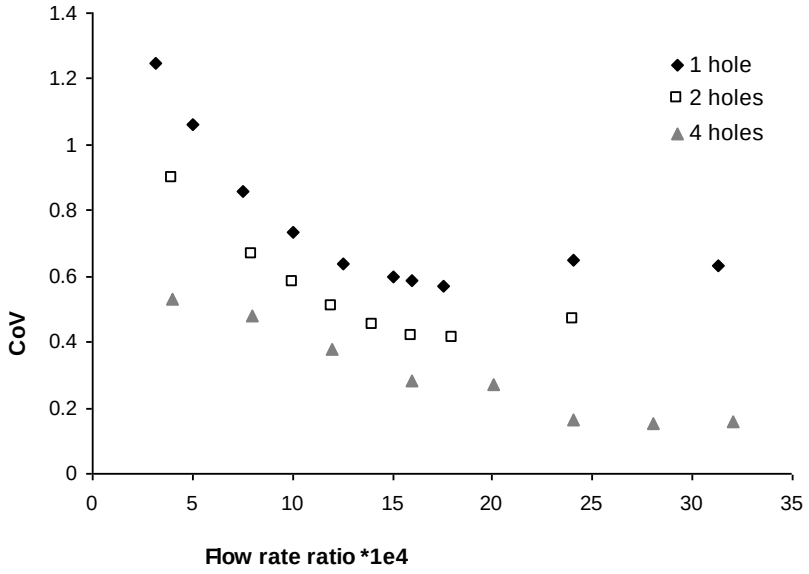

Figure 4-9: Coefficient of variance for a pipe with D_{in}=10mm and D_m=1m

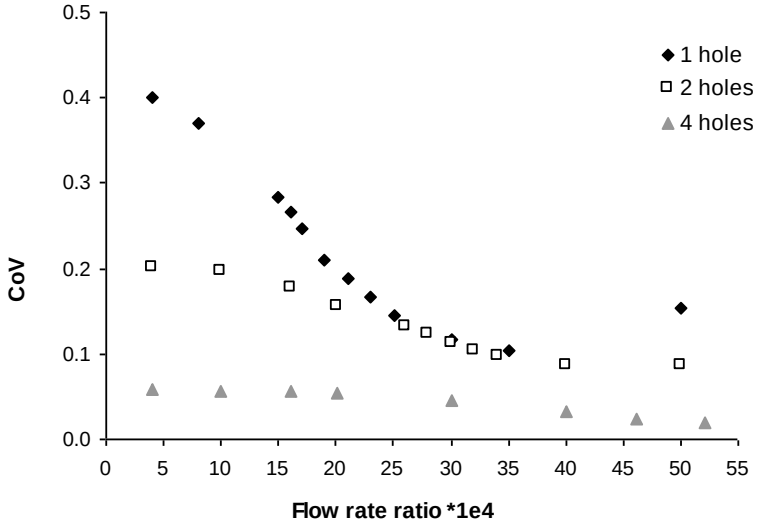

Figure 4-10: Coefficient of variance for a pipe with D_{in}=10mm and D_m=0.5m

Below are the same three graphs except that the CoV is plotted versus the momentum ratio instead.

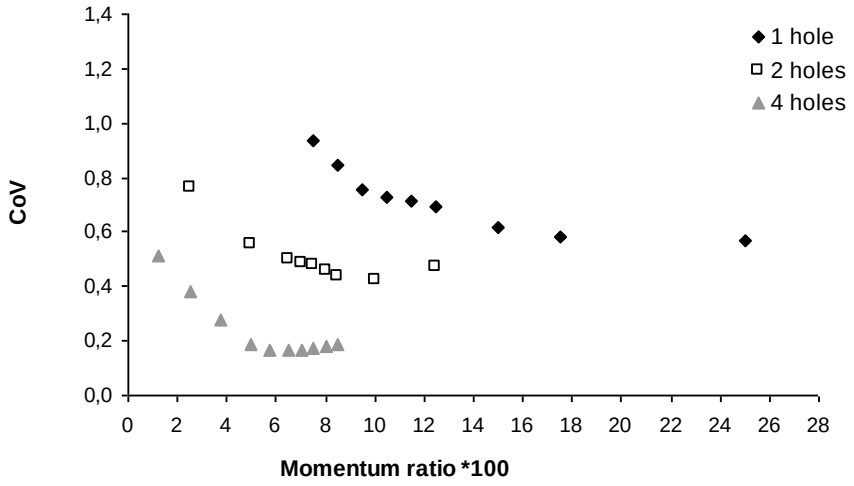

Figure 4-11: Coefficient of variance for a pipe with D_{in}=5mm and D_m=1m

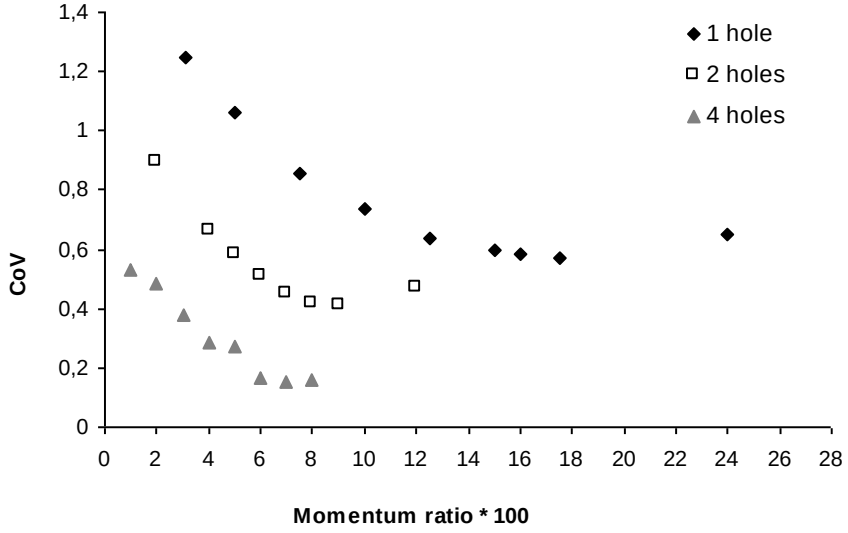

Figure 4-12: Coefficient of variance for a pipe with D_{in}=10mm and D_m=1m

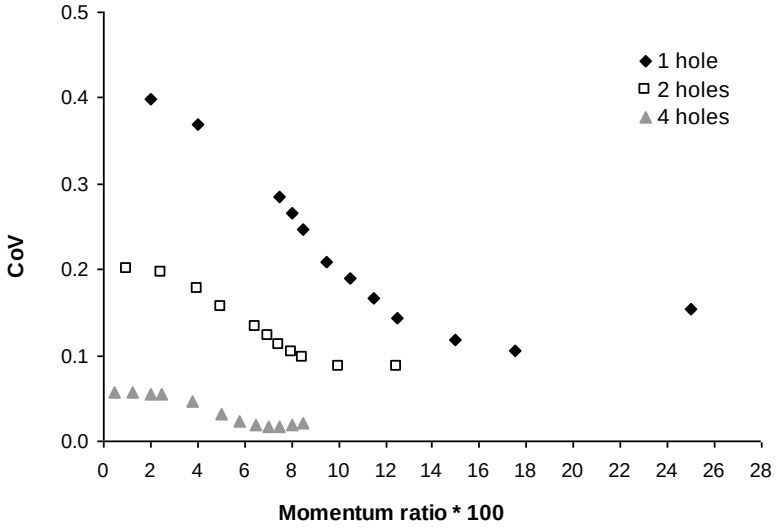

Figure 4-13: Coefficient of variance for a pipe with D_{in}=10mm and D_m=0.5m

4.4.1 Velocity vectors

Velocity vectors for a flow rate ratio of approximately $25 \cdot 10^4$ for 1, 2 and 4 injection points are viewed in Figure 4-14 to 4-16. It is for a pipe with D_{in}=10mm and D_m=1m. Here the rotation around the injection points can be seen 1 m downstream of the injection. Notice that for 4 injection points the rotation caused by the injection does not affect the flow in the middle of the pipe. The scale up of the velocity vectors is 2000 for all three figures.

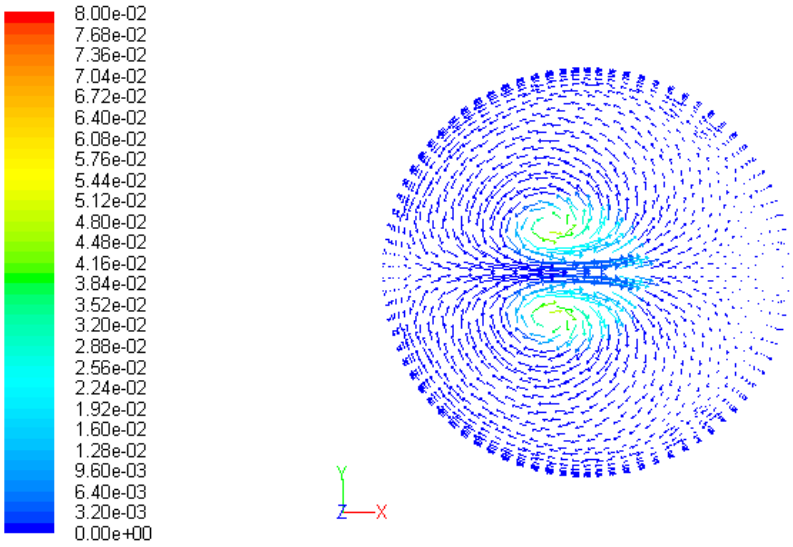

Figure 4-14: Velocity vectors colored by mass fraction, 1 injection point

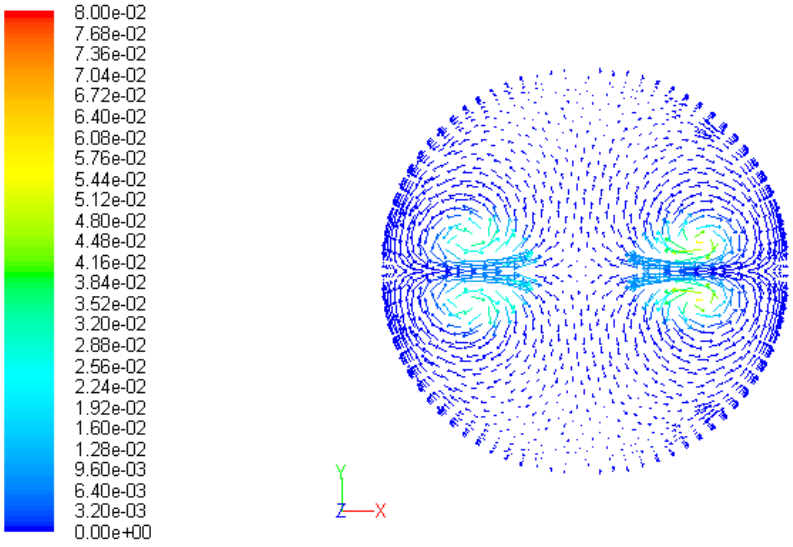

Figure 4-15: Velocity vectors colored by mass fraction, 2 injection points

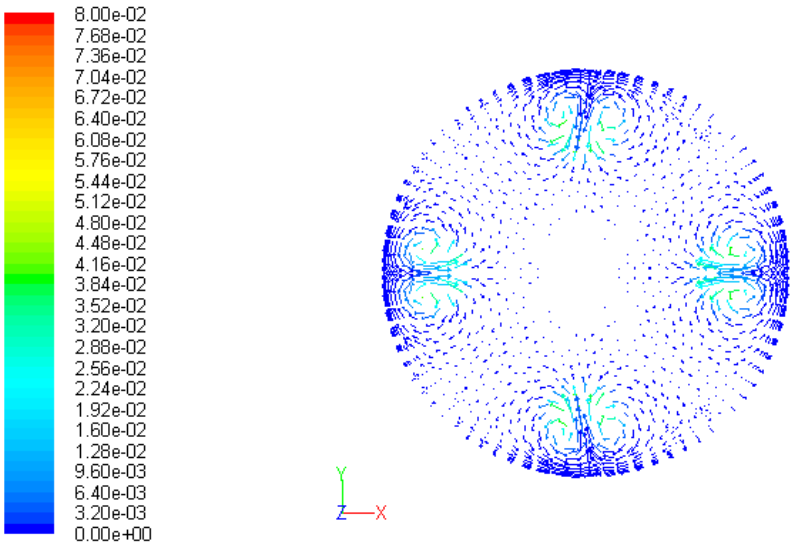

Figure 4-16: Velocity vectors colored by mass fraction, 4 injection points

In Figure 4-17 the mass fraction of injected species for a cross section 10m downstream of the injection is presented. This is for the same cases as showed in fig 4-14 to 4-16. The arrows in the bottom of the figure show the direction of the injections.

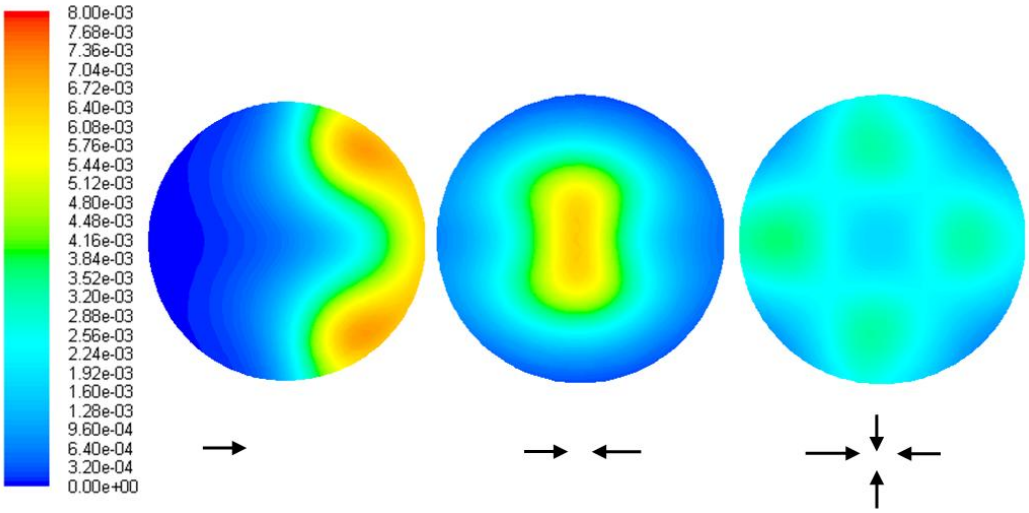

Figure 4-17: Mass fraction of injected species 10m downstream of injection

Rheology model dependency

The Coefficient of Variance is calculated from a cross section 10m from injection to compare the rheology models. The results from the simulations with a single injection point are given in Figure 4-18.

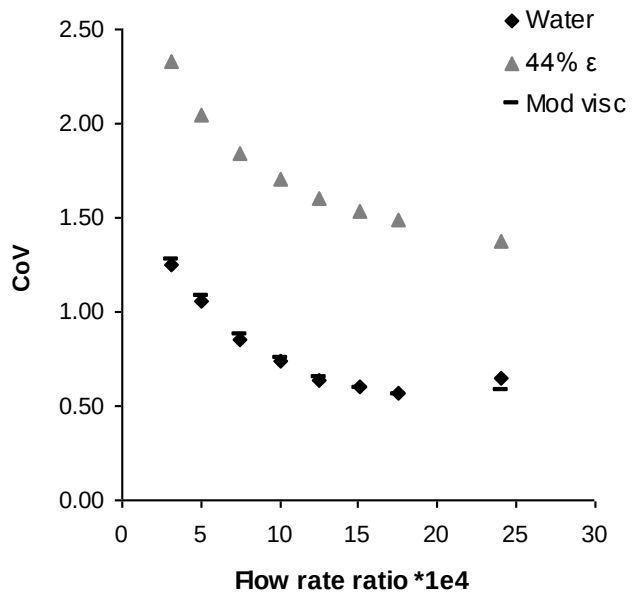

Figure 4-18: Coefficient of variance for 1 injection point

Turbulence model dependency

In Figure 4-19 to 4-21 the Coefficient of Variance is calculated for a cross section 10m downstream from injection for simulations with Standard k-ε model, RNG k-ε model and RSM. The result points missing in the graphs are due to problems with convergence caused by instabilities at high velocities for the RNG k- ε model and RSM.

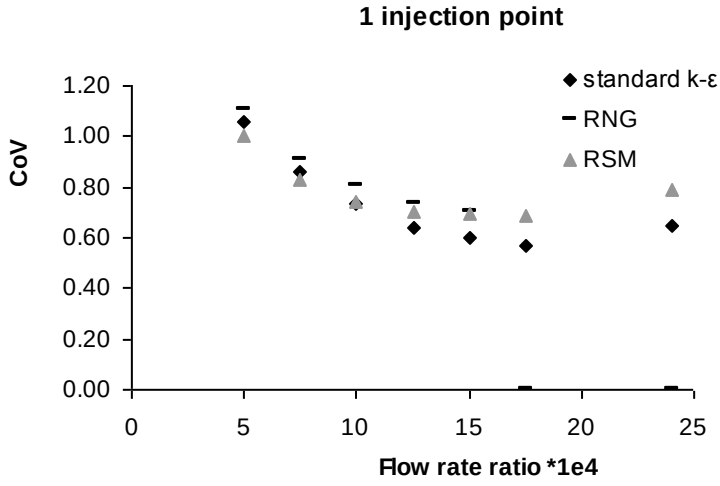

Figure 4-19: Study for 1 injection point with the Standard k-ε model, the RNG k-ε model and RSM.

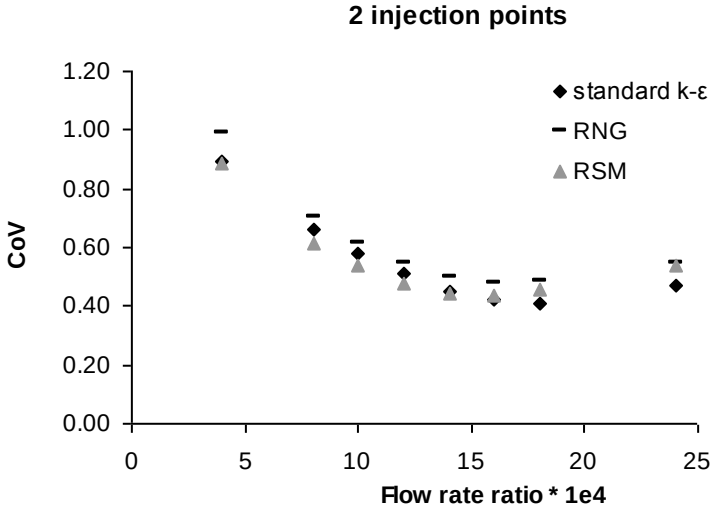

Figure 4-20: Study for 2 injection points with the Standard k-ε model, the RNG k-ε model and RSM.

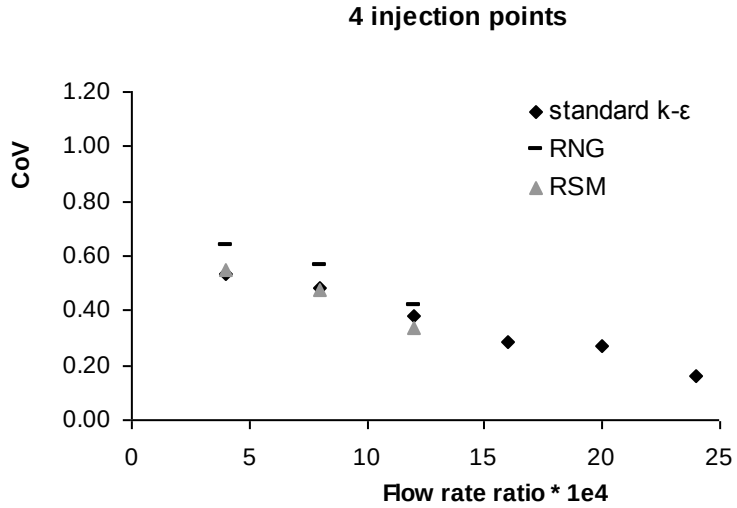

Figure 4-21: Study for 4 injection points with the Standard k-ε model, the RNG k-ε model and RSM.

RSM gives a higher CoV for high velocity injections than the Standard k-ε model does. When mesh refinements are performed the CoV is changing in the same direction for both the Standard k- ε model and RSM.

Grid dependency

The solutions are not grid independent. However the grid dependency was mainly significant for high injection velocities. The current grid dependency was accepted due to the larger uncertainty of the suspensions rheology.

Generally refinement leads to decreased numerical diffusion, but in the performed simulations it also caused an increased turbulent intensity. For low injection velocities the refinement led to an increased CoV due to that the reduced numerical diffusion of species dominated. For high injection velocities the refinement led to reduced CoV due to that the increased turbulent viscosity was dominating. Refinements for the velocity gradient and concentration gradient gave results in the same direction.

5 Discussion

5.1 Movement and effects of individual fibers and flocks

Kolmogorovs length scale which represents the smallest eddies is from 0.03 to 0.08 mm for a water simulation. For the fibers there is a size distribution but a general fiber size is approximately 0.5 -2 mm. The smallest eddies are thus in the order of a centesimal of the main fibers, and therefore most of the fibers will not follow the smallest eddies. The nanoparticles in the retention chemicals on the other hand will follow the eddies and the viscous-diffusive phenomenon will transport the nanoparticles to the fiber surface. The turbulence will also transport fines and fillers to the fibers. If the fibers would follow the smallest eddies like the nanoparticles, fines and fillers the molecular diffusion would have to transport the nanoparticles, fines and fillers to the fibers and that transport time would be in the order of minutes.

Since the turbulence can transport the nanoparticles all the way to the fiber surface it is very important with a fast macro mixing to avoid an uneven distribution of the nanoparticles. However, the inertial convective time scale is the larger for the pipe flows with water and hence it is the limiting time scale. This is the large scale mixing. The viscous diffusive time scale, which is mixing on the smallest scale, is the fastest.

The turbulent Stokes number is around 1 for the flocks and their effect can therefore be neglected for the generation of turbulence. The flocks' effect on the dissipation should however not be neglected.

5.2 Rheology models

Water

When studying the results from measurements performed on turbulent channel flow with PUDV presented in chapter 2.4.3, the best approximation seems to be to simulate the system as pure water. At a Reynolds number of 90 000 the dependency of concentration is significantly reduced. If this would be extrapolated it could be believed that the turbulent intensity would be almost unaffected by the concentration at a Reynolds number of 2 000 000. This is the Reynolds number for the mesh used for the base case simulated with water.

The following uncertainties should be mentioned. The method only measures the movements of the fiber phase and not the movement of the water phase. Technically the situation could be that the turbulence in the water phase is damped while only the fibers are moving in a similar way at the different concentrations. That is however not probable. It is also unclear how the zero point is measured since PUDV only can measure fibers and not water. The slowness of the measurement with PUDV should also be kept in mind.

Apparent viscosity

It was expected that the injection depth would be shorter for injection into a fluid with high viscosity. A tendency of a decreased penetration depth could be seen in the case with modified viscosity. At high injection velocities the inertial force is large compared to the viscous force and the viscous force can then be neglected. Therefore

the effect of increased viscosity was larger for lower injection velocities, but it was still negligible.

It is unlikely that the apparent viscosity would be this high in a turbulent flow. The graph in Figure 2-3 only shows the dependency on the shear rate and not on the Reynolds number. It is not likely that flows with different Reynolds numbers have the same apparent viscosity simply because the flows have the same mean shear rate.

Reduced ε

The model with reduced ε gives a too low pressure drop. This means that too little energy is added to the system. The Reynolds number is not known for the measurements and the reduced dissipation rate in the experiments does not mean that the energy is reduced in the whole system. Probably the energy is mainly lost to fiber interactions on small length scales in the size of the fibers. In the suspension there will not be a balance between the added energy to the suspension and the energy dissipated leading to mixing in the water phase. To simulate this as a one phase system and assuming that the dissipation is halved is therefore an underestimation of the turbulence. To use experimental data for a tank with impeller when simulating a pipe flow is also very uncertain.

Uncertainty in measurements

Since the methods available are either not fast enough or not intrusive enough to measure in a turbulent fiber suspension there is no reliable experimental data available for systems similar to the system to be studied. No measurements have been performed for Reynolds numbers of 2 000 000. Whether the turbulence in a suspension completely would merge with the properties of a pure water system for sufficiently high Reynolds numbers has not been reported in any literature found.

How turbulent the studied system actually is can vary. It can be misleading to get too focused on a fully turbulent pipe flow with a Re 2 000 000 since it is unlikely that it would have time to develop. It is important not to mix in chemicals close downstream of the screen if injection with TEE nozzles is utilized. Having a screen close upstream to the injection means a not so turbulent regime. It takes up to 40 meter for a fully turbulent profile to develop in water. For a suspension at low Reynolds number the slip of the fiber phase will cause that it takes longer time for the velocity profile to develop, but for a suspension at high Reynolds numbers the slip is negligibly small.

5.3 Turbulence model dependency

The Standard k-ε model results in lower CoV than RSM does at high injection rates. The turbulent viscosity is overestimated for the Standard k-ε model. The turbulent viscosity has lower gradients in the standard k-ε model case, it is smoother. This could be due to the fact that Standard k- ε fails when there are rapid changes in mean shear rate.

Generally the RNG k-ε model is excluded since it is known to be inferior to the Standard k-ε model for jet injection. However, it was tested but it was hard to reach convergence with RNG. Its results were not closer to RSM than the Standard k-ε models results were.

5.4 Degree of mixing

In chapter 2.3 a rough indication of the degree of mixing is given. The CoV should be below 0.1 or 0.2 for the mixing to be good and a CoV below 0.05 is defined as completely mixed. The following CoV could be reached for simulations with water but how close it is to the CoV in reality is uncertain. For a pipe with a diameter of 1m the completely mixed condition could not be reached with the injection configurations tested. A CoV below 0.2 could be reached with 4 injection points for a pipe with a diameter of 1m and a flow rate ratio of 0.25%. For the pipe with a diameter of 0.5m a CoV of 0.05 could be reached with 4 injection points for a flow rate ratio of 0.4%. That a smaller pipe can reach a lower CoV is both because the injections can cover a larger part of the pipe and because the turbulent properties of the flow are different.

Four injection points showed to be better than 1 and 2 for all geometries tested and all rheology models. That 4 injection points is better than 1 and 2 does not mean that the more injection points the better since the injections affect each other's rotation and since the injection depth per injection point is reduced for the same total injection flow rate.

6 Conclusions

The injection depth can be approximated by the momentum ratio. An increased injection depth gives reduced CoV. This decrease in CoV starts for a momentum ratio around 3%. For 4 injection points the CoV only decreases until a momentum ratio of around 6%, but for 2 injection points it decreases until a momentum ratio of approximately 8% and for 1 injection point until a momentum ratio around 12%. By reducing the diameter of the injection nozzle a larger injection depth can be reached with the same injection volume flow.

4 injection points is better than 1 and 2 for all three rheology models and all geometries tested.

Water is the closest estimation of the rheology models used. Still it can be good to keep the modified viscosity model and the reduced dissipation rate model in mind since the turbulence at injection varies at different plants for example due to the distance to the screen. It takes 30 to 40 meters to develop a velocity profile in water and in a suspension it takes either the same distance or longer. A less turbulent flow is more damped and hence gets even less turbulent.

6.1 Further work

More measurements are needed in the semi concentrated regime at high Reynolds numbers. To do this, better techniques needs to be developed to measure the turbulent fluctuations at high Reynolds numbers and concurrently be intrusive enough.

Since 4 injection points tends to damp each other's circulation around the injection for high injection velocities it could be interesting to instead place injection points after each other downstream. If the injection points have the right distance downstream they could amplify each other's circulation.

To have a pipe bend is one way to increase the mixing. Since it is a turbulent flow there will be a plug flow, and the plug might also be more distinct due to the fibers. Since there is a plug the velocity will be approximately the same in the whole pipe except for a few millimeters closest to the pipe wall. The effect of a pipe bend will hence be smaller than for a laminar flow, but could still increase the mixing to some level.

It could also be of interest to simulate a smooth hinder in the pipe. After the hinder there will be a circulation due to the expansion of the cross section. If the circulation is adapted to the circulation caused by the injection these circulations could amplify each other. When designing the smooth hinder the risk for buildup of particles needs to be thoroughly considered.

References

1. M. A. Hubbe, 'Flocculation and redispersion of cellulosic fiber suspensions: A review of effects of hydrodynamic shear and polyelectrolytes', *BioResources,* Vol. 2(2), 2007, pp. 296-331.

2. C. da Silva Santos, 'New mixing technology for Wet End Improves Environmental Performance', *Pulp and paper magazine*, 2007

3. J. Matula, 'Immediate and efficient mixing of wet end additives close to PM headbox', in Wet End Technologies, January 2010, viewed on 14 January 2010, <http://www.wetend.com/media/Close_to_headbox.pdf>

4. H. Holik, 'Paper and Pulp – Paper and Board Manufacturing', *Ullmans Encyclopedia*, Wiley-VCH Verlag Gmbh & Co. KGaA, Weinheim, 2005

5. B. Andersson, R. Andersson, L. Håkansson, M. Mortensen, R. Sudiyo, B. von Wachem, *Computational Fluid, Dynamics for Chemical Engineers,* 5th edition, Chalmers, Göteborg, Sweden, 2009

6. L. J. Forney, 'Jet injection for optimum pipeline mixing', *Encyclopedia of Fluid Mechanics Vol. 2 Dynamics of Single-Fluid Flows and Mixing*, Nicholas P. Cheremisinoff, Gulf Publishing Company, Huston, Texas, 1986, pp. 660-690.

7. L.M. Sroka, and L.J. Forney, 'Fluid mixing with a pipeline TEE: Theory and experiment', *AIChE J*, Vol. 35(3), 1989, p. 406-414. Found in [8]

8. G. Pan, H. Meng, *An Experimental Study of turbulent mixing in a Tee Mixer Using PIV and PLIF*, Laser Flow diagnostics laboratory, Dept. of Mechanical & Aerospace Engineering, Atate Univeristy of New York at Buffalo, Buffalo, NY 14260, 2001.

9. C. Cozewith, M. Busko, 'Design correlation for Mixing Tees', *Ind. and Eng. Chem. Res.*, Vol. 28, 1521, 1989. Found in [8]

10. G. Tosun, 'A Study of Micromixing in Tee Mixers', *Ind. and Eng. Chem. Res.*, Vol. 26, 1184, 1987. Found in [8]

11. C. P. J. Bennington, J. P. MMbaga, *Liquid phase turbulence in pulp fiber suspensions*, The University of British Columbia, Vancouver, BC, Canada, 12th Fundamental Research Symposium, Oxford, September, 2001.

12. S. R. Andersson, *Network disruption and turbulence in fiber suspensions*, Department of Chemical engineering design, Chalmers University of technology, Göteborg, Sweden, 1998, p. 14f.

13. R. J. Kerekes, 'Rheology of fiber suspensions in papermaking: An overview of recent research', *Nordic Pulp and Paper Research Journal*, Vol. 21, no. 5, 2006.

14. H. Fock, *The flow of pulp suspensions, experimental and numerical studies*, Chalmers University of technology, Göteborg, Sweden, 2009

15. A. Rasmuson, Professor, Chalmers University of Technology, Göteborg, 2009-12-09

16. T. Wikström, *Flow and rheology of fiber suspensions at medium consistency*, Department of Chemical Engineering Design, Chalmers University of Technology, Göteborg, Sweden, 2002.

17. J. R. Welty, C. E. Wicks, R. E. Wilson, G. L. Rorrer *Fundamentals of momentum, heat, and mass transfer*, 3rd edition, John Wiley & Sons, Hoboken, USA, 1984, p. 497.

18. J. Gullishen, E. Härkönen, 'Medium consistency technology – I.', *Fundamental data*, Tapi 59(8), pp. 115-122, 1981. In [14]

19. D. Hammarström, *A model for simulation of fiber suspension flows*, KTH mechanics, Royal institute of technology, Stockholm, 2004

20. G. G. Duffy, L. Abdullah, Fiber Suspension Flow in Small Diameter Pipes, Appita J. Vol. 56(4), 290-295. Found in [13]

21. S. Dong, X. Feng, M. Salcudean, I. Gartshore, 'Concentration of pulp fibers in 3D turbulent channel flow', *International Journal of Multiphase Flow*, Vol. 29 1-21, 2003.

22. D. Hammarström, J. P. Hämäläinen, A. Dahlkild, A. Jäsberg, *Modeling of Laminar Suspension Flows*, submitted to Computers and Fluids, 2003. Found in [1].

23. D. Hammarström, J. P. Hämäläinen, A. Dahlkild, A. Jäsberg, *Modeling of Turbulent Suspension Flows*, submitted to 'Computers and Fluids', 2003. Found in [1].

24. J. X. Hanjiang, K. A. Cyrus, 'Characteristics of fiber suspension flow in a rectangular channel', *International journal of multiphase Flow*, Vol. 31, 2005.

25. J. A. Pettersson, *Flow and mixing of pulp suspension*, Chalmers University of science, Göteborg, Sweden, 2004, p. 31.

26. R. J. Kerekes, R. G. Garner, 'Measurement of Turbulence in Pulp Suspensions by Laser Anometry', *Trans. Tech. Sect. CPPA*, 8, TR53-TR60, 1982. In [25]

27. M. Steen, 'The Application of Refractive Index Matching for Two-phase Flow Measurements in Turbulent Fiber suspensions by Laser Doppler Anemometry', Nord. *Pulp Pap. Res. J.*, 4(4), pp. 236-243, 1989. In [25]

28. M. Steen, 'On Turbulence Structure in Vertical Pipe Flow of Fiber Suspensions', *Nord. Pulp Pap. Res. J.*, 4(4), pp. 244-252, 1989. In [25]

29. F. Lundell[1], D. Söderberg[1,2], S. Storey[3], R. Holm[1], *The effect of fibers on laminar-turbulent transition and scales in turbulent decay*, [1]KTH Mechanics, Stockholm, Sweden, [2]STFI Packfors AB, Stockholm, Sweden, [3]University of British Columbia, Vancouver, Canada

30. D. C. Wilcox, *Turbulence Modeling for CFD,* 3rd edition, DCW Industries Inc., California, 2006

31. A. O. Demijrent, 'Multigrid acceleration and turbulence models for computations of 3D turbulent jets in crossflow', *Int. J. Heat Mass Transfer*, Vol. 35. No. 11. pp.2 783-2794, 1992

32. Ansys Fluent 12.0, Users guide

33. C. Crowe, M. Sommerfeld, Y. Tsuji, *Multiphase Flows with Droplets and Particles,* CRC Press LLC, Florida, USA, 1998

34. M. Sommerfeld, B. van Wachen, R. Oliemans, *Best Practice Guidelines for Computational Fluid Dynamics of Dispersed Multiphase Flow,* ERCOFTAC, 2008

Used software

A. Gambit 2.4.6

B. ANSYS inc., Fluent 12.0

Appendix 1: Create geometry and mesh

Create geometry

1. Create a cylinder in the z-direction, with the center of the inlet in origo.
2. Create circles with their center point in (x,y,z)=(0,0,1). One in the xz-plane and one in the yz-plane.
3. Project the circles on the envelope surface of the cylinder. Project in positive and negative x- and y direction.
4. Make a plane through the pipe on the length and one cross plane on each side of the injection (10cm from the injection).
5. Split the volume, first on the length and then split the injection volume from the rest and then split the holes from the rest.

Create mesh (for base mesh)

1. The edges representing a half circle have an edge spacing of 0.04.
2. Boundary layers are created for the surfaces (including the 3 holes and the 3 envelope surfaces of the half cylinder). First layer = 0.002, growth factor = 1.4, number of layers = 7.
3. The injection holes with a diameter of 10mm have an edge spacing of 0.003. The holes are then meshed. (Ca 20 mesh faces)
4. A size function from the holes and into the volume is created. Smallest size 0.001, growth factor 1.4, maximum volume = 0.04.
5. The "injection volume" is meshed with size 0.04. TGrid meshing scheme needs to be used for this volume.
6. The two other volumes are meshed with size 0.05. Cooper scheme is used. When meshing the volume closest to the inlet, the inlet area should be first in the list of source faces to get a good boundary layer. When meshing the volume closest to the outlet, the outlet area should be first in the list of source faces.

Wall functions

Standard wall functions were used for all cases. This was because the bulk flow was much larger than the injected flow. Therefore the injections effect could be neglected in the near wall area.

The boundary layer was created so the y+ value was below 100.
The mesh created for a bulk flow velocity of 6m/s had the following boundary layer:
First layer = 0.001, growth factor = 1.4, number of layers = 7

Appendix 2: User defined function to modify the viscosity

```
#include "udf.h"
#define R 0.5
#define water 0.001003
#define appvisc 0.14

DEFINE_PROPERTY(visc,c,t)
{
        real u[3];
        real x, y, z, r;
        real ny;

                C_CENTROID(u,c,t);
                x = u[0];
                y = u[1];
                z = u[2];
                r = pow(pow(x,2.0) + pow(y,2.0),0.5);

                if (r > 0.485)
                        ny = water+(R-r)*13.8997;
                else
                        ny = appvisc;

        return ny;
}
```